THE ANNALS OF "DUNAREA DE JOS" UNIVERSITY OF GALATI
FASCICLE V, TECHNOLOGIES IN MACHINE BUILDING,
ISSN 2668-4829 (PRINT) 2668-4888 (ONLINE)
https://doi.org/10.35219/tmb.2025.1.10

ANALYSIS OF THE FUNCTIONALITY OF A LINEAR HYDRAULIC MOTOR IN A LOW-PRESSURE HYDROSTATIC SYSTEM

Elena Felicia BEZNEA[1], Andrea MIRON[1],
Florin CHIRIȚĂ[2], Nicușor BAROIU[3,4]

[1] Mechanical Engineering Department, "Dunarea de Jos" University of Galati, Romania
[2] Chif Technology SRL, Bucharest, Romania
[2] Department of Manufacturing Engineering, "Dunarea de Jos" University of Galati, Romania
[3] Research Center in Manufacturing Engineering Technology (ITCM), "Dunarea de Jos" University of Galati, Romania
email: Nicusor.Baroiu@ugal.ro

ABSTRACT

The document proposes the analysis and design of a low-pressure hydrostatic drive system, an area of interest from the perspective of resource optimization and technological performance improvement, with reference to the analysis of the functionality of a linear hydraulic motor.

The way fluids transfer energy is examined, with an emphasis on essential hydrostatic calculations such as determining transmitted speeds and forces. These principles will form the basis for simulations performed using OMEGON Fluid software, which will facilitate the visualization and optimization of assembly diagrams.

Another main aspect is the design and analysis of a linear hydraulic motor, using CAD tools and FEM methods, studying the mechanical behavior of the motor, and identifying how stress and deformations are distributed under load.

KEYWORDS: Hydraulic system, low pressure, linear hydraulic motor, OMEGON Fluid, CAD, FEM.

1. INTRODUCTION

Hydrostatic driven systems play a crucial role in transmitting mechanical energy through fluids, being frequently used in various industrial fields due to their reliability and versatility. These systems convert mechanical energy into hydraulic energy and then reconvert it into mechanical energy to generate linear or rotational motion [1]. Thus, they include a set of interconnected components designed to precisely and efficiently control and direct the flow of fluid to achieve optimal mechanical performance.

This feature makes them extremely effective in applications that require high forces and precise movement.

Numerous and varied studies have been conducted in this regard on low-pressure systems, both in terms of low working pressure (usually below 50 bar, sometimes even below 20 bar) and the fluids used, or specific components: low-flow pumps, appropriately sized hydraulic motors, or other control elements designed for low-pressure regimes or for low-pressure compensation [2,3].

The pressure losses and the behavior of a check valve at low pressures were studied. A revelant study for the design of passive components in low-pressure systems is presented in [4]. Various practical solutions for low-pressure pumping units have also been proposed, such as the use of miniboosters to generate higher pressure pulses starting from initially low-pressure systems [5].

Multi-pressure architectures have been proposed to optimize energy efficiency, suitable for mobile applications or equipment where some parts of the circuit can operate at low pressures [6].

The analysis of a low-pressure hydrostatic drive system, performed using specialized software tools

such as OMEGON Fluid, allows the identification of interdependencies between the main operating parameters — pressure, flow rate, and power — under varying load conditions. The simulations facilitate the optimization of the system configuration and contribute to reducing energy losses and increasing the functional efficiency of the installation [7].

Another common element of study consists of the design and analysis of structural components of hydrostatic systems, using CAD modeling tools and finite element analysis (FEM) methods to study structural behavior under load. Within these stages, the distributions of stresses, deformations, and critical areas of the assembly can be identified [8,9]. The results of these analyses allow a better understanding of the interaction between hydraulic forces and the mechanical strength of the structure, optimizing the geometry and materials for hydraulic components and contributing to improving the performance and reliability of the system [10,11].

The hydraulic cylinders are linear motors that convert the hydrostatic energy of the working fluid into mechanical translational energy, characterized by force and speed. In low-pressure applications (below ~50 bar), they are used in light mechanisms, laboratory equipment, automation, or auxiliary systems where controlled movements are required, but not high forces.

Under the same low-pressure conditions, cylinders are optimized to reduce internal losses and ensure tightness at low pressures, using elastic materials and low-roughness surfaces, and are available in a wide variety of designs (Figure 1).

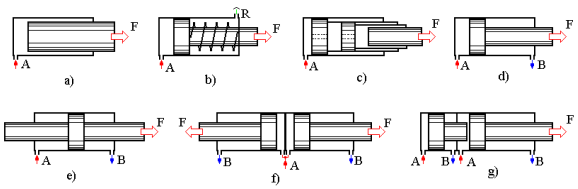

Fig. 1. *Types of hydraulic cylinders*

2. CHARACTERISTIC PARAMETERS. CALCULATION FORMULAS

Low-pressure cylinders are often integrated into circuits with small-capacity pumps and proportional flow control valves for precise control.

Also, the main features of low-pressure hydraulic cylinders are the efficient operation of seals at low pressures, as well as the manufacture of components from light alloys (aluminum, composite materials), while still maintaining structural rigidity.

Hydraulic deceleration at the end of the stroke is achieved by finely throttling the flow to prevent shocks even under low pressure conditions.

The main design parameters are: working pressure (p), which is low, below 10 bar in most cases; developed force (F), proportional to pressure and piston area; flow rate (Q), which determines the speed of rod movement (v).

Volumetric and mechanical efficiencies are low (η_v, η_m) at low pressures, due to internal leaks.

In these applications, the cylinders are designed for short strokes and moderate speeds, avoiding high dynamic loads.

The average speed of the piston movement is calculated using the following formula:

$$v = \frac{Q}{S}, \tag{1}$$

where:

S - effective piston area;

Q - the value of the oil flow rate entering the hydraulic cylinder.

The liquid flow rate required in the cylinder is calculated using the following formula:

$$Q = \frac{S \cdot v}{\eta_v}, \tag{2}$$

where:

η_v - volumetric efficiency.

A simple hydrostatic drive system (low pressure) with a hydraulic cylinder as the actuating element, is shown in Figure 2.

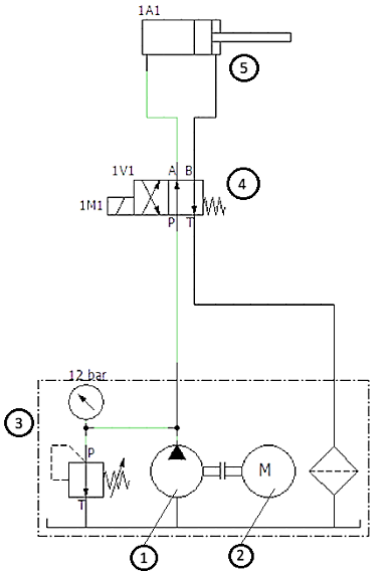

Fig. 2. *The operating principle of a hydrostatic system, in OMEGON Fluid*

The operation of the system is based on the circuit being supplied by a pump driven by an electric motor (*2*).

The generated flow is directed through a safety valve (*3*) and controlled by a 4/2 distributor (*4*).

Depending on its position, the fluid is directed either to chamber *A* or chamber *B* of the linear hydraulic motor (*5*). Thus, the piston moves in one direction or the other, performing the necessary mechanical movement. When the distributor returns to the neutral position, the circuit is discharged, and the piston movement stops.

3. ANALYSIS OF THE HYDRAULIC MOTOR

3.1. Experimental research

To determine the main operating parameters of the linear hydraulic motor, such as force and speed, it is necessary to know some construction and working parameters, such as piston diameter, rod diameter, stroke, and working pressure. These parameters are presented in Table 1, and Figure 3 provides a graphical representation of the linear hydraulic motor, useful for understanding its structure and operating principle.

Table 1. *Technical characteristics of the motor*

Cylinder type	Linear, double-effect
Piston diameter, *D* [mm]	20
Rod diameter, *d* [mm]	10
Stroke [mm]	58
Viscosity [mm²/s]	10...100

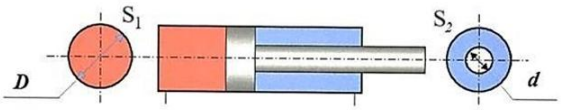

Fig. 3. *Graphical representation of the hydraulic cylinder*

In order to standardize calculations, the standardized values shall be adopted, as follows:

- pressure, $p = 2, 4, 6, 8, 10$ [bar];
- flow rate, $Q = 0.43; 0.55; 0.67; 0.8; 0.86$ [l/min].

The determination of the force developed by the motor is based on the fundamental relationship between pressure, force, and area, expressed by the formula:

$$p = \frac{F}{S} \rightarrow \mathrm{F} = p \cdot S \tag{3}$$

Depending on the active part of the piston, area *S* differs. Thus, for the solid part of the piston (without rod), the effective surface area is:

$$S_1 = \frac{\pi \cdot D^2}{4} \tag{4}$$

For the rod part, the active surface area is reduced by the cross-sectional area of the rod, resulting in:

$$S_2 = \frac{\pi \cdot \left(D^2 - d^2\right)}{4} \tag{5}$$

Table 2. *Motor pressure and force values (F_1)*

p = [bar]	F = [daN]	
$p_1 = 2$	$F_1 = p_1 \cdot S_1 \cdot 10^{-2}$	= 6,28
$p_2 = 4$	$F_3 = p_2 \cdot S_1 \cdot 10^{-2}$	= 12,56
$p_3 = 6$	$F_5 = p_3 \cdot S_1 \cdot 10^{-2}$	= 18,84
$p_4 = 8$	$F_7 = p_4 \cdot S_1 \cdot 10^{-2}$	= 25,12
$p_5 = 10$	$F_9 = p_5 \cdot S_1 \cdot 10^{-2}$	= 31,4

Table 3. *Pressure and motor force values (F_2)*

F = [daN]	
$F_2 = p_1 \cdot S_2 \cdot 10^{-2}$	= 4,71
$F_4 = p_2 \cdot S_2 \cdot 10^{-2}$	= 9,42
$F_6 = p_3 \cdot S_2 \cdot 10^{-2}$	= 14,13
$F_8 = p_4 \cdot S_2 \cdot 10^{-2}$	= 18,84
$F_{10} = p_5 \cdot S_2 \cdot 10^{-2}$	= 23,55

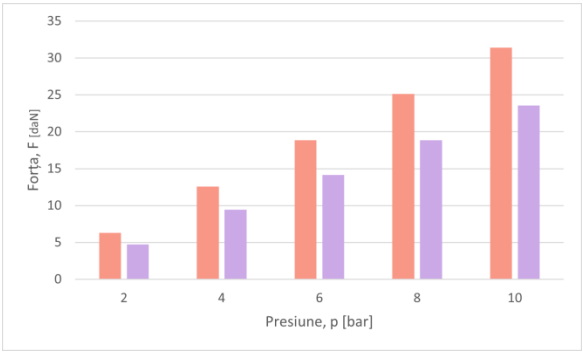

Fig. 4. *Graphical representation of pressure and velocity*

To evaluate the dynamic behavior of the linear hydraulic motor, it is essential to determine the speed at which the piston moves under the action of the fluid.

The speed calculation starts from the general relationship (*2*), which takes into account *Q* - the volume flow rate of the fluid [l/min], v - the piston speed [m/s], and *S* - the active surface area on which the fluid acts [mm²]. By reformulating this relationship, we obtain the expression for velocity (*1*).

Table 4. *Flow rate and motor speed (v_1) values*

Q = [l/min]	v = [m/min]	
0,43	$v_1 = \frac{Q_1}{S_1} \cdot 10^3$	= 1,36
0,55	$v_3 = \frac{Q_2}{S_1} \cdot 10^3$	= 1,75
0,67	$v_5 = \frac{Q_3}{S_1} \cdot 10^3$	= 2,13
0,8	$v_7 = \frac{Q_4}{S_1} \cdot 10^3$	= 2,54
0,86	$v_9 = \frac{Q_5}{S_1} \cdot 10^3$	= 2,73

Table 5. *Flow rate and motor speed (v_2) values*

v = [m/min]	
$v_2 = \frac{Q_1}{S_2} \cdot 10^3$	= 1,82
$v_4 = \frac{Q_2}{S_2} \cdot 10^3$	= 2,33
$v_6 = \frac{Q_3}{S_2} \cdot 10^3$	= 2,84
$v_8 = \frac{Q_4}{S_2} \cdot 10^3$	= 3,39
$v_{10} = \frac{Q_5}{S_2} \cdot 10^3$	= 3,65

Calculations will be performed for several distinct values of piston speed, corresponding to standardized flow rates, the results being specified in Tables 4 and 5, and Figure 5.

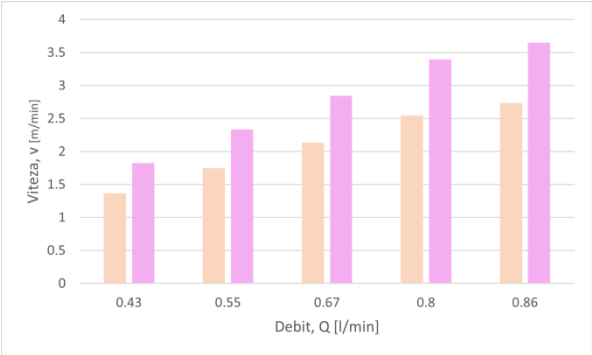

Fig. 5. *Graphical representation of flow and velocity*

The calculations performed for the linear hydraulic motor allowed the determination of the generated force and the piston displacement speed for different combinations of pressure and flow, using expressions derived from the fundamental principles of hydraulics.

3.2. Parameter configuration in OMEGON Fluid

For the simulation performed in OMEGON Fluid to reflect the real behavior of a low-pressure hydrostatic drive system, it is essential to correctly configure each component element with precise data.

The parameters describing the system components—from the pump to the distributor, cylinder, pipes, and protective elements—have a direct influence on the results obtained in the simulation, both from a kinematic and a functional and energy perspective.

The hydraulic cylinder is double-acting and has the following characteristics configured in Omegon:

- Piston diameter: 20 mm;
- Rod diameter: 10 mm;
- Stroke: 58 mm;
- Average force: 14 N;
- Average speed: 2.50 m/min.

These dimensions were entered into the software to accurately reproduce the linear movement of the rod during simulation. The cylinder was connected directly to the hydraulic distributor via rigid pipes to ensure control of the direction of movement.

Figure 6 shows the initial operating state when the electrical control that controls the distributor is activated. This switches the internal position and allows the oil flow from the pump to pass to one of the chambers of the hydraulic cylinder. As a result, the piston rod begins to move outwards.

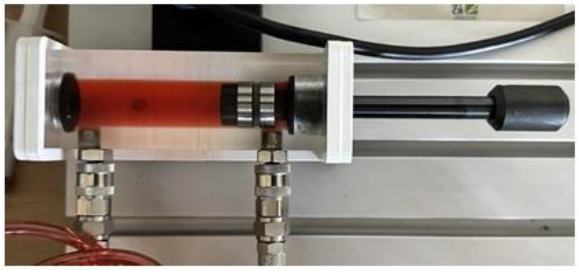

Fig. 6. *Controlled displacement of the cylinder rod during the forward stroke*

As the simulation progresses, as seen in Figure 7, the flow continues to feed the cylinder, and the rod movement occurs in a controlled manner, supported by constant oil pressure. The electrical control is maintained throughout the stroke, ensuring a complete working cycle.

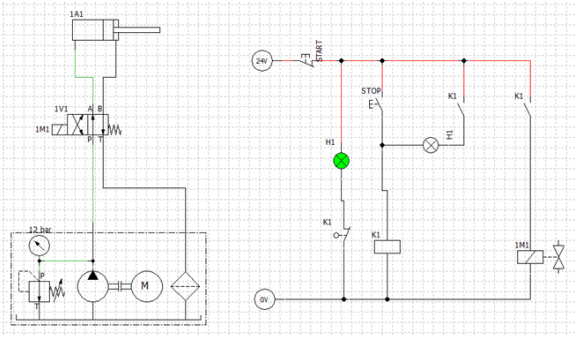

Fig. 7. *Simulation in OMEGON Fluid, advance stroke*

In this phase, the pressure in the circuit increases with the mechanical load, and this phenomenon is also confirmed by the reading on the pressure gauge attached to the pump unit.

During the active stroke of the cylinder, the pressure gauge records a value of approximately 4.2 bar. This value corresponds to the working pressure developed at that moment in the circuit, in accordance with the specifications of the designed low-pressure system.

Once the electrical control is interrupted, the distributor automatically returns to its neutral position, Figure 8, according to the internal configuration.

This condition is illustrated in Figure 9, where the connections between the pump and cylinder are broken and the oil is directed back to the reservoir.

At this point, the piston rod remains stationary, marking the end of a complete operating cycle of the system.

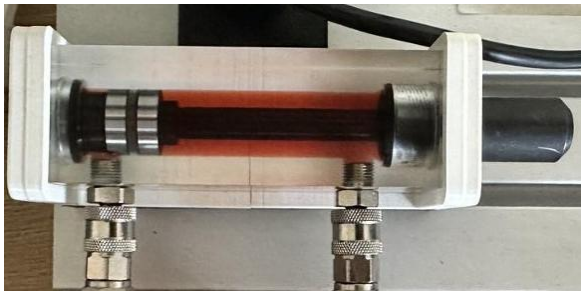

Fig. 8. *Controlled movement of the cylinder rod during the retraction stroke*

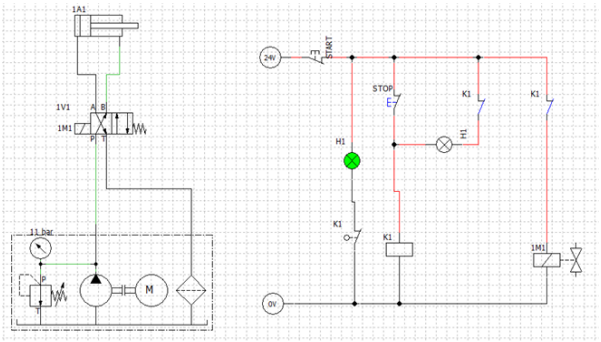

Fig. 9. *Simulation in OMEGON Fluid, retraction stroke*

Once the stroke is complete, the pressure in the system progressively decreases, and the pressure gauge gradually returns to its initial value, indicating a state of hydraulic rest.

To investigate the dynamic behavior of the hydrostatic drive system, an analysis of the main signals obtained from the simulation performed in the OMEGON Fluid environment was performed.

A synchronized evolution of the distributor control and the position of the hydraulic cylinder rod defines four complete cycles of advance and retraction, with a periodic sequence of movements, each cycle lasting approximately 4 seconds, which indicates the stability and repeatability of the system's operation.

The distributor switches and supplies the corresponding pressure chamber, determining the advance stroke of the rod. When the signal returns, the direction of fluid flow is reversed, causing the cylinder to retract completely.

The results show a precise correlation between the distributor control and the movement of the hydraulic actuator, confirming the automatic and stable operation of the system. The synchronization of the signals validates the correctness of the implemented control logic and demonstrates the system's ability to perform repetitive cycles with constant advance and retract times without dynamic instabilities.

4. CAD MODEL AND FEM ANALYSIS

The modeling began by drawing cross-sections of the main components of the hydraulic motor: the outer cylinder, the piston, the covers, and the fluid inlet and outlet channels.

These entities were then extruded and assembled virtually to obtain the complete geometry of the motor.

All dimensions were chosen in accordance with the values resulting from the calculations, ensuring a realistic and functional geometry.

To better highlight the internal structure and fluid flow channels, a wireframe (realistic) view was generated, illustrated in Figure 10.

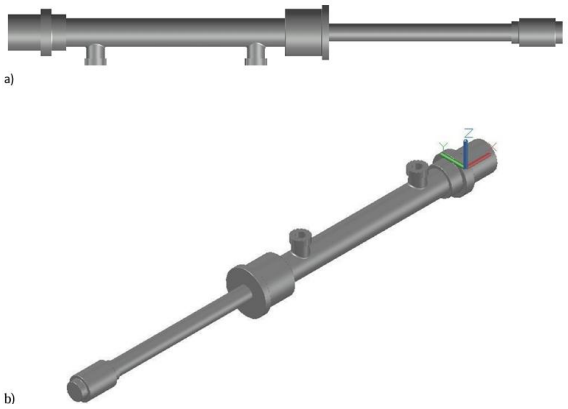

Fig. 10. *a) Front view; b) Isometric view of the linear hydraulic motor*

After completing the CAD model, the linear hydraulic motor geometry was exported in STEP (*.step*) format, a standard format that preserves the three-dimensional solid details required for simulation.

This file was subsequently imported into the Ansys Workbench platform for structural analysis.

Within the *Engineering Data Sources and Engineering Data* modules, it was necessary to assign a material corresponding to the geometric model (Figure 11).

Since the hydraulic motor analyzed is made of steel, the material Stainless Steel was selected.

This material has suitable mechanical properties for components subject to internal pressure stress.

In the *Design* module, the geometry was preliminarily analyzed to verify the integrity of the surfaces, the continuity of the volumes, and any possible import errors

Since the objective of the simulation was to study the structural behavior of the cylinder shell under internal pressure, components that did not significantly influence this stress – such as the piston rod – were eliminated before the FEM analysis.

This simplification of the model was intended to reduce the complexity of the calculation without compromising the accuracy of the results.

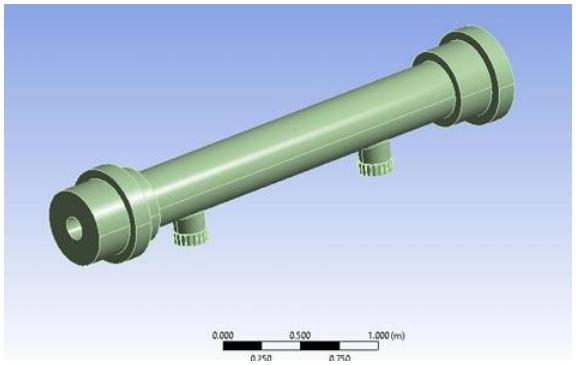

Fig. 11. *Hydraulic motor preprocessed in Ansys Workbench*

4.1. Definition of FEM analysis conditions

After importing, validating, and preparing the geometric model in *Ansys*, the necessary conditions for performing the structural finite element analysis were defined.

For local control of element size and fine discretization, the *Face Sizing* condition was applied to the lateral face of the cylinder shell represented in Figure 12, setting the element size value to 0.1 m.

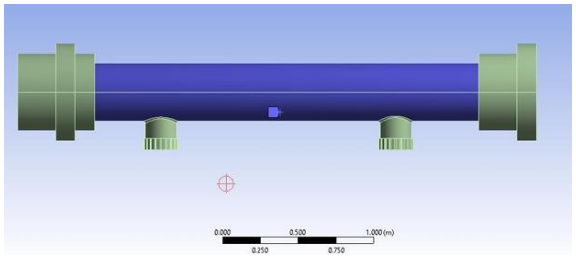

Fig. 12. *Application of the Face Sizing condition on the side face of the motor*

Face Sizing control ensures uniform discretization on the selected face, preventing the generation of distorted or disproportionate elements.

After applying the settings for the finite element mesh, the final mesh of the hydraulic motor model was generated, as shown in Figure 13. The resulting mesh has a balanced density with no errors or distorted elements identified.

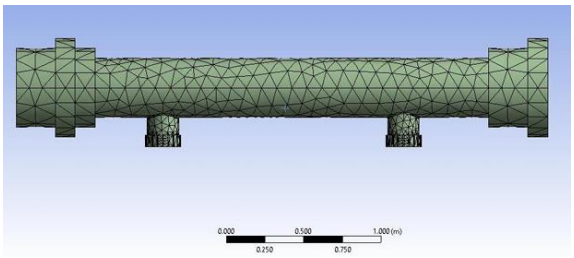

Fig. 13. *The result of the mesh*

To simulate as accurately as possible the structural behavior of the hydraulic motor housing under real operating conditions, the *Fixed Support* condition was defined in the analysis.

The fixings were applied to:

- the circular faces of the cylinder side covers;
- the outer surfaces of the two suction and discharge ports, as shown in Figure 14.

In these regions, all six degrees of freedom were canceled, thus preventing any rigid movement of the assembly during pressure application.

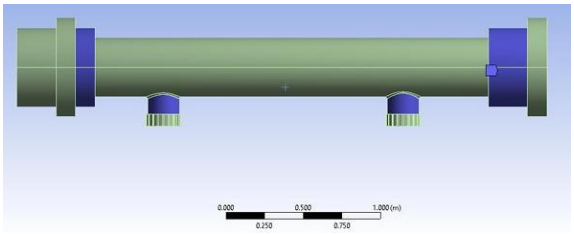

Fig. 14. *Fixed Support conditions applied to engine surfaces*

To reproduce the real operating conditions of the hydraulic motor, a uniformly distributed internal pressure was applied to the inner surface of the cylinder.

This pressure simulates the effect of the hydraulic fluid on the inner walls of the housing during a stationary operating cycle. The pressure application surface was the inner cylindrical part of the motor.

Figure 15 shows the geometric model after the application of the load, indicating the area on which the defined pressure acts.

The pressure values used in the analysis were chosen based on the hydraulic parameters calculated previously. Based on these, five pressure values were used, p = (2, 4, 6, 8, 10) bar.

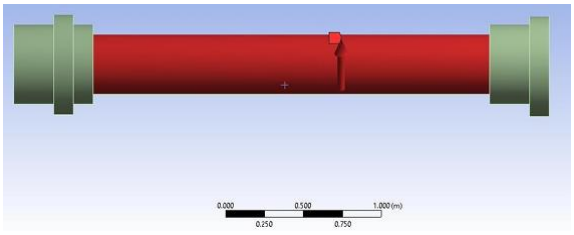

Fig. 15. *Applying internal pressure to the internal surface of the engine*

4.2. Analysis of the results obtained by the FEM method

For each case, the equivalent stress (von Mises) and total displacement were analyzed to verify whether the structure withstands the stresses within the limits imposed by the material and to identify any critical areas.

The results obtained from the analysis indicate extremely low values of displacements, specific to the elastic behavior of the material.

As the pressure increases, the total deformation gradually increases.

Table 6 summarizes the maximum values of the total displacement depending on the analyzed pressure.

Table 6. *Maximum values of total displacement*

Nr. ctr.	Presiune, p [bar]	Deplasare maximă, [m]
1.	2	$2{,}34 \cdot 10^{-7}$
2.	4	$4{,}68 \cdot 10^{-7}$
3.	6	$7{,}02 \cdot 10^{-7}$
4.	8	$9{,}37 \cdot 10^{-7}$
5.	10	$1{,}17 \cdot 10^{-6}$

Figure 16 visually highlights how deformation manifests itself in the model structure. This is true both for the 2-bar pressure shown in the image and for the other pressures analyzed.

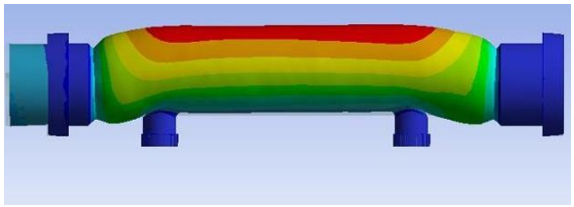

Fig. 16. *The total displacement of the engine*

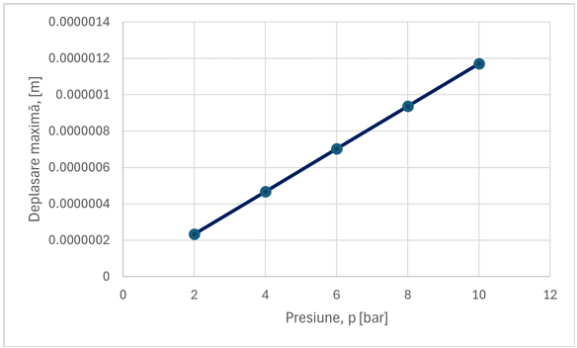

Fig. 17. *Graphical representation of total displacement*

The graph in Figure 17 illustrates the variation of maximum deformation as a function of the applied internal pressure.

An almost linear relationship between pressure and displacement is observed, specific to an elastic behavior of the structure.

The results show that the linear hydraulic motor exhibits small and progressive displacements under the action of pressure, without exceeding the allowable limits.

To evaluate the internal stresses, the FEM analysis followed the distribution of von-Mises equivalent stresses in the cylinder, at the same pressure values.

The results obtained show a proportional increase in maximum stress with applied pressure, without exceeding the critical threshold.

Table 7 summarizes the maximum values of the equivalent stresses recorded.

Table 7. *Maximum stress values*

Nr. ctr.	Presiune, p [bar]	Tensiune echivalentă max. [MPa]
1	2	0,727
2	4	1,45
3	6	2,18
4	8	2,91
5	10	3,63

Fig. 18. *Von Mises stress of the motor*

Figure 19 shows the distribution of equivalent von Mises stresses in the linear hydraulic motor cylinder for all pressure values.

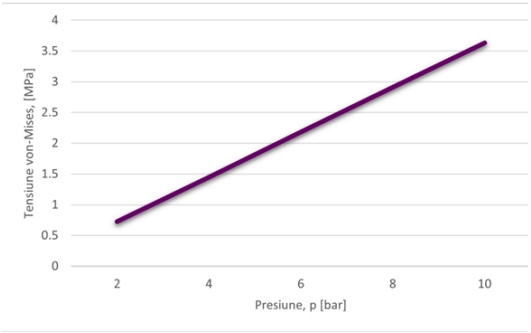

Fig. 19. *Graphical representation of von Mises stress*

The graph in Figure 19 shows a linear relationship between the pressure applied inside the cylinder and the equivalent von Mises stress.

The maximum value obtained, 3.63 MPa at 10 bar, is significantly below the material's yield strength, indicating high structural strength and operational safety.

The distribution of the safety factor shown in Figure 20, following the analysis, with values between 1 and 15, indicates that the entire engine body is within the strength limits.

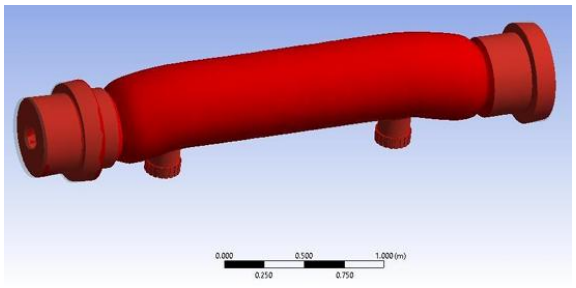

Fig. 20. *Representation of the safety factor for the engine*

The dominant red areas suggest a safe working regime without the risk of reaching the material's yield limit.

The minimum safety factor value is 1, which shows that at the most stressed point, the equivalent stress reaches the material's yield limit.

However, this threshold is not exceeded, which confirms that the engine can operate under maximum load conditions without danger of structural failure.

To highlight the influence of the material on the structural behavior, the analysis of the same hydraulic motor was redone, replacing the stainless steel with an aluminum alloy.

All other conditions were kept identical. The purpose of this approach is to compare the structural response of the assembly when using a lighter but less rigid material.

Table 8. *Maximum stress and displacement values*

Nr. ctr.	Presiune, p [bar]	Deplasare maximă, [m]	Tensiune maximă, [MPa]
1	2	$5{,}88 \cdot 10^{-7}$	0,789
2	4	$1{,}17 \cdot 10^{-6}$	1,41
3	6	$1{,}76 \cdot 10^{-6}$	2,12
4	8	$2{,}35 \cdot 10^{-6}$	2,83
5	10	$2{,}94 \cdot 10^{-6}$	3,54

a)

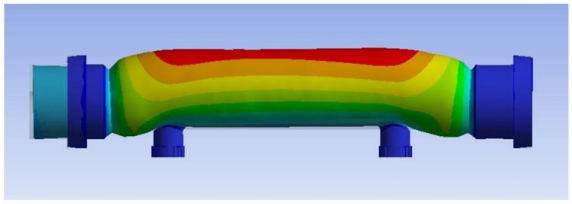

b)

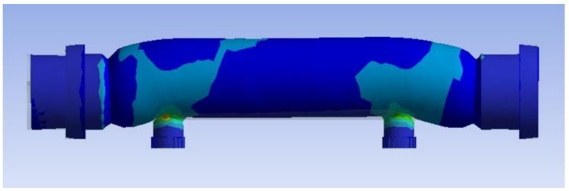

Fig. 21. *a) Maximum displacement; b) Maximum von Mises stress*

According to Table 8, the the analysis results performed on the engine indicate a progressive increase as the internal pressure increases.

The results of the analysis are also clearly presented in Figure 21(a, b). The total deformation of the assembly shown in Figure 21(a) has a significant increase in the maximum displacement relative to the steel. In Figure 21(b), the distribution of the von-Mises equivalent stresses is visible, located mainly in the connection area between the cylinder and the inlet/outlet ports.

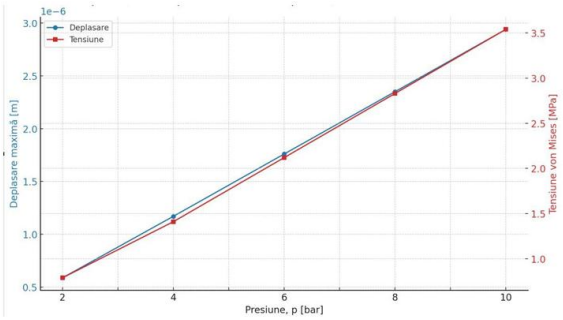

Fig. 22. *Graphical representation of displacement and maximum stress*

The graph shown in Figure 22 highlights how the maximum displacement and stress increase proportionally with the applied pressure, the body being made of aluminum.

A linear evolution is observed for both quantities, which indicates an elastic behavior specific to the analyzed material.

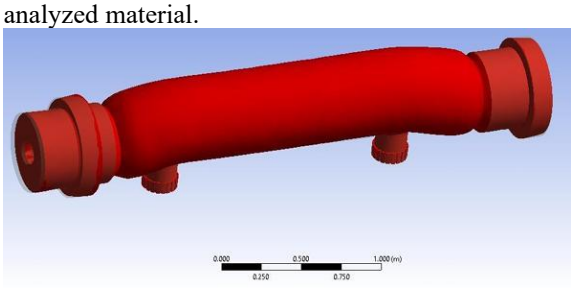

Fig. 23. *Representation of the safety factor for the motor (material: aluminum)*

Figure 23 shows the result of the safety factor analysis for the motor made of aluminum.

The value approaching the lower threshold of 1 indicates that, in certain areas, the generated stresses are comparable to the yield strength of the material.

Although aluminum remains elastic for the pressures analyzed, the low safety factor indicates a lower margin of safety. Thus, the material can be used successfully but requires greater attention in design to avoid local overloads.

The hydraulic motor model will be structurally analyzed using gray cast iron as the base material, a material known for its high rigidity and compressive strength. This choice aims to highlight the behavior of a more fragile, but dimensionally stable material, compared to the options previously analyzed.

Table 9. *Maximum displacement and stress values for cast iron*

Nr. ctr.	Presiune, p [bar]	Deplasare maximă, [m]	Tensiune maximă, [MPa]
1	2	$4{,}56 \cdot 10^{-7}$	0,75
2	4	$9{,}13 \cdot 10^{-7}$	1,50
3	6	$1{,}37 \cdot 10^{-6}$	2,25
4	8	$1{,}82 \cdot 10^{-6}$	3,00
5	10	$2{,}28 \cdot 10^{-6}$	3,75

The values obtained are shown in Table 9, and they indicate a progressive increase in both displacement and von Mises stress as the applied pressure increases.

The maximum stress remains below the yield strength of the material.

The distribution of the obtained results can also be observed in the images below, which illustrate the total displacement and equivalent stress field for the applied pressures.

This representation in Figure 24(a, b) validates the values in the previous table and highlights the elastic behavior of the cast iron motor.

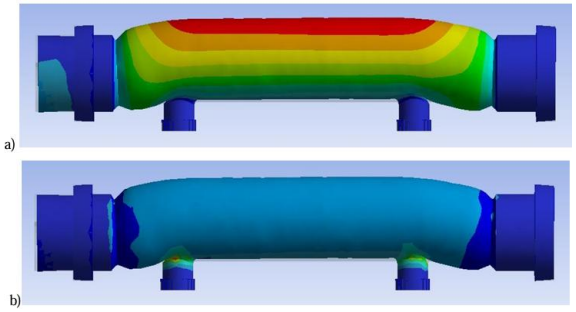

Fig. 24. *a) Maximum displacement for cast iron engine; b) Maximum von Mises stress*

The graphs in Figure 25 illustrate the structural behavior of the engine housing made of cast iron, under the action of internal pressures ranging between 2 and 10 bar.

A progressive increase of both quantities is observed as a function of pressure, specific to the elastic regime.

The total displacement is maintained within reduced limits, confirming the characteristic rigidity of cast iron, while the equivalent von-Mises stress increases almost linearly, without exceeding the yield strength of the material.

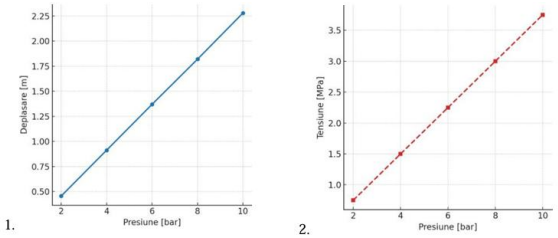

Fig. 25. *Graphical representation: 1) displacement; 2) stress*

Figure 26 illustrates the result of the safety factor analysis for the hydraulic motor made of cast iron.

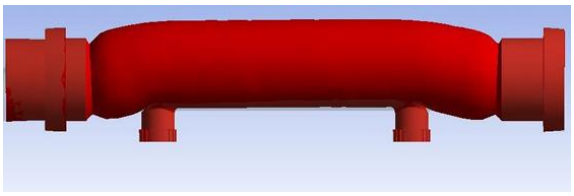

Fig. 26. *Representation of the safety factor for the motor (material: cast iron)*

The very low highlighted values indicate that the part is at the limit of its resistance capacity under working pressure.

This distribution suggests increased structural vulnerability, and the material does not provide an adequate safety margin for reliable continuous operation.

Thus, from the point of view of safety, durability, and behavior under internal stresses, steel represents the superior option for the construction of the hydraulic motor analyzed.

5. CONCLUSIONS

The mechanical and economic advantages of a low-pressure hydraulic system derive not only from reduced component wear due to moderate pressures but also from minimized energy losses and ease of maintenance.

By analyzing this system in detail, it is proposed not only to understand its theoretical functioning but also to create a functional model that reflects real performance.

The choice of material for a hydraulic motor is not only dictated by mechanical behavior, but also by economic efficiency.

The raw material cost directly influences the final price of the product, and the ratio between performance and price becomes essential.

If an analysis is made of the approximate purchase values for the three materials analyzed together with an estimate of their share in industrial use, especially in the field of drive systems and hydraulic component construction, it could be concluded that:

- Stainless steel offers the best mechanical performance and a high safety factor but comes with the highest purchase cost. It is recommended for demanding applications where reliability and service life are critical.
- Aluminum is moderately priced and has good machinability. Although less rigid, it is effective in applications where weight is a factor. It is a good compromise between cost, mass, and performance.
- Cast iron is the most affordable material, but its structural behavior limits its use to static applications with moderate loads. It can be chosen where cost is

the main criterion, but no compromises are made in terms of safety.

The results showed significant differences between the three materials in terms of deformability, von Mises equivalent stresses, and safety factor.

Stainless steel offered the most stable performance, with minimal deformation and a high safety margin, making it ideal for demanding applications.

Aluminum stood out for its low weight and moderate cost, but with lower rigidity. Aluminum is recommended for applications where low weight and flexibility are essential, while steel is more suitable where stability and minimal deformation under mechanical stress are required.

Cast iron, although economical, presented more obvious structural limits, having a minimal safety factor at high pressures.

The analysis was completed by evaluating economic efficiency, where it was demonstrated that the choice of material must take into account both mechanical performance and acquisition, processing, and availability costs.

The modeling and simulations performed provide a complete picture of the functional behavior of the motor and support informed decision-making in the design of a low-pressure hydraulic drive system.

REFERENCES

[1] Baroiu, N., Teodor, V.G., Costin, G.A., *Constructive-functional analysis of single-rod double-acting hydraulic cylinders*, *Tehnomus J. - New Tech. and Prod. in Mach. Manuf. Tech.*, 126-131, 2017.

[2] Costin, G.A., Afteni, C., Iacob, I., Păunoiu, V., Baroiu, N., *An overview on sheet metal hydroforming technologies*, *The Ann. of "Dunarea de Jos", Univ. of Galați, Fasc. V, Tech. in Mach. Building*, ISSN 2668-4829, 36:55-62, 2018;

[3] Lu, G., Wang, Z., Fan, L., Gu, Y., Xu, J., Wu, Y., Xiao, Y., *Research on the pressure fluctuations and hydraulic resonance phenomena in the high-pressure pipelines of marine common rail systems*, Energy, 313, 133975, 2024.

[4] Carpintero, J., Martinez, B., Fábregas, J., Pérez, J., Canales, F., *Hydraulic characterization of a check valve for low-pressure potable water distribution applications,* Water, 15, 2475, 2023.

[5] Popescu, T.C., Chiriță, A.P., Nieśpiałowski, K., Popescu, A.M.C., *Method and means of measuring pulsating flowrates of oscillating hydraulic pressure intensifiers*, Proceedings of International Conference on Hydraulics and Pneumatics – HERVEX, ISSN 1454 – 8003, 2023.

[6] Xu, Z., Bertolin, M., Vacca, A., Nilsson, J., *A hydraulic architecture based on multi-common pressure rail principle using multi-chamber cylinders for excavators*, Advancements in Fluid Power Technology: Sustainability, Electrification, and Digitalization. GFPS 2024. Lecture Notes in Mechanical Engineering. Springer, 2025.

[7] Omegon Fluid, https://en.omesim.com/

[8] Baroiu, N., Moroșanu, G.A., Graphical modelling and studies on hydraulic pump parameters, *J. of Ind. Design and Eng. Graph.* - JIDEG, 15(2):7-12, 2020.

[9] Kodirov, D., Tursunov, O., *Modeling and analysis of a reactive low-pressure hydraulic turbine*, IOP Conf. Ser.: Mater. Sci. Eng., 883, 012085, 2020.

[10] Baroiu, N., Moroșanu, G.A., Teodor, V.G., Crăciun, R.S., Păunoiu, V., *Use of reverse engineering techniques for inspecting screws surfaces of a helical hydraulic pump*, *Int. J. of Modern Manuf. Tech.*, XIV(2):20-29, 2022.

[11] Belabend, S., Păunoiu, V., Baroiu, N., Khelif, R., Iacob, I., Boazu, D., *Static Structural Analysis Analytical and Numerical of Ball Bearings*, IOP Conf. Series: Materials Science and Engineering 968, 012026, 2020.

[12] Baroiu, N., Moroșanu, G.A., Miron, A., Moroșanu, F.I., Chiriță, F., *Analysis of a low-pressure hydrostatic drive system,* Proceedings of the International Conference on Hydraulics, Pneumatics, Sealing Elements, Precision Mechanics, Tools, Specific Electronic Equipment & Mechatronics - HERVEX 2025, pp. 36-48, ISSN 1454-8003, 2025.